Hough Parameter Space Regularisation for Line Detection in 3D

Manuel Jeltsch[1], Christoph Dalitz[1] and Regina Pohle-Fröhlich[1]
[1]*Institute for Pattern Recognition, Niederrhein University of Applied Sciences, Reinarzstr. 49, 47805 Krefeld, Germany*
manuel.jeltsch@gmail.com, {christoph.dalitz, regina.pohle}@hsnr.de

Keywords:
Hough transform, 3D line detection, ridge detection, laser scan data.

Abstract:
The Hough transform is a well known technique for detecting lines or other parametric shapes in point clouds. When it is used for finding lines in a 3D-space, an appropriate line representation and quantisation of the parameter space is necessary. In this paper, we address the problem that a straightforward quantisation of the optimal four-parameter representation of a line after Roberts results in an inhomogeneous tessellation of the geometric space that introduces bias with respect to certain line orientations. We present a discretisation of the line directions via tessellation of an icosahedron that overcomes this problem whenever one parameter in the Hough space represents a direction in 3D (e.g. for lines or planes). The new method is applied to the detection of ridges and straight edges in laser scan data of buildings, where it performs better than a straightforward quantisation.

1 INTRODUCTION

Originally proposed for line detection in a 2D space (Hough, 1962), the Hough transform has meanwhile become a standard tool for detecting a wide variety of parametric shapes (Mukhopadhyay and Chaudhuri, 2015). Unlike other shape detection algorithms, the Hough transform does not work on images, but on point clouds. Its application to images thus requires a preprocessing step for filtering candidate points. The idea of the Hough transform is to consider each candidate point as a "vote" for all predefined shapes to which it might belong. The predefinition of the shapes is done by a discretisation of the parameter space. Shapes with many points will then get many votes in the parameter space.

Time and space complexity of the Hough transform not only depend on the size of the point cloud, but also on the dimension of the parameter space and the coarseness of the parameter discretisation. For ellipse detection in 2D, e.g., the parameter space is five dimensional, and there have been a number of suggestions for making this problem more tractable (Mukhopadhyay and Chaudhuri, 2015). For line detection in 2D, lines are typically represented with the Hessian normal form, which results in a two dimensional parameter space. In three dimensions, the Hessian normal form does not represent lines, but planes, and a straightforward generalisation of the original Hough transform to 3D thus leads to plane detection with a three dimensional parameter space (Ishida et al., 2012).

For line detection in 3D, an appropriate parametric line representation needs to be chosen. The text book line representation is the vector form $\vec{a} + t\vec{b}$, where $\vec{a}$ is a point on the line and $\vec{b}$ (with $\|\vec{b}\| = 1$) is the direction of the line. Even though this line representation is redundant and leads to a five dimensional parameter space, it has indeed been used for line detection with the Hough transform (Moqiseh and Nayebi, 2008). One way to reduce the space and time complexity is a hierarchical approach that first searches for peaks in the slope parameter space, which is only two dimensional, and to further investigate these peaks in the intercept parameter space, which is two dimensional too (Bhattacharya et al., 2000).

A different way to reduce the complexity is to use a non-redundant line representation, thereby reducing the number of dimensions. A minimal and optimal representation of a line with four parameters was given by Roberts (Roberts, 1988; Schenk, 2004). This representation has already been used for needle detection in 3D ultrasonic images (Zhou et al., 2008; Qiu et al., 2013).

In the present paper, we show that a straightforward discretisation of Roberts' parameter space leads to an inhomogeneous sampling pattern that favours certain directions. To overcome this shortcoming, we suggest a discretisation of two parameters, namely the angles specifying the normal vector of Roberts' plane through the origin, by means of a sphere tessellation. As a use case, we apply the new method to edge detection in laser scan data, where the candidate points are prefiltered based on the local curvature in the point cloud. In our experiment, the new approach lead to better results than a straightforward discretisation with the same number of parameter cells.

This paper is organised as follows: in section 2, we give a general description of the Hough transform, introduce Roberts' line representation and our parameter space discretisation. In section 3, we describe how the method can be used to detect arbitrarily oriented ridges and other straight edges in 3D laser scan data.

2 LINE DETECTION IN 3D

Before we specialise the Hough transform for 3D line detection, let us first describe the Hough transform in its most general case, and then discuss the problems of 3D line representation and its parameter space discretisation.

2.1 Hough transform

Let $X = \{\vec{x}_1, \ldots, \vec{x}_n\}$ be a point cloud in which we look for curves defined by k parameters and described in the parametric form

$$f(\vec{x}, p_1, \ldots, p_k) = 0 \tag{1}$$

For a given list of parameters $p_1, \ldots, p_k$, all points $\vec{x}$ on the curve fulfil Eq. (1). The basic idea of the Hough transform is to consider this equation not as a condition for $\vec{x}$, but for the parameters $p_1, \ldots, p_1$: all curves to which a given point belongs are given by all parameter values that fulfil Eq. (1). Generally, the number of possible curves

Algorithm 1 Hough transform

```
Input: point cloud $X = \{\vec{x}_1, \ldots, \vec{x}_n\}$, parameter
    values $P_i = \{p_{i1}, \ldots, p_{iN_i}\}$ for $0 < i \leq k$
Output: voting array $A$ of size $N_1 \times \ldots \times N_k$
 1: $A(p_1, \ldots, p_k) \leftarrow 0$ for all $p_1, \ldots, p_k$
 2: for $\vec{x} \in X$ do
 3:   for $p_1 \in P_1$ do
 4:     ...
 5:     for $p_{k-1} \in P_{k-1}$ do
 6:       $p' \leftarrow g(\vec{x}, p_1, \ldots, p_{k-1})$    ▷ cf. Eq. (2)
 7:       $p_k \leftarrow$ nearest neighbour to $p'$ from $P_k$
 8:       $A(p_1, \ldots, p_k) \leftarrow A(p_1, \ldots, p_k) + 1$
 9:     end for
10:     ...
11:   end for
12: end for
13: return A
```

is infinite, but it can be made finite by a discretisation of the parameter space: each parameter p_i is assumed to be limited to a range of N_i values from a finite set $P_i = \{p_{i1}, \ldots, p_{iN_i}\}$, where the number N_i of possible parameter values may vary from parameter to parameter.

Each of the discrete parameter values then represents a cell in parameter space, and a point $\vec{x}$ votes for all cells that contain parameters fulfilling Eq. (1). To make the voting process tractable, Eq. (1) must be rewritten as

$$g(\vec{x}, p_1, \ldots, p_{k-1}) = p_k \tag{2}$$

Then all parameter cells, to which $\vec{x}$ belongs, can be determined in a loop over all parameter values $P_1 \times \ldots \times P_{k-1}$ and by computing the cell of the last parameter through Eq. (2). The resulting algorithm is listed as Algorithm 1.

2.2 Line parametrisation

For the purpose of algorithmic efficiency it is advisable to use a parametrisation that is unique, does not suffer from singularities and is non-redundant. Such a parametrisation for lines in 3D that uses only four parameters (x', y', ϕ, θ) was given by Roberts (Roberts, 1988).

The *direction* of a line can be specified by the two parameters ϕ for horizontal orientation (*azimuth*) and θ for altitude (*elevation*) (see Fig. 1). The directional vector $\vec{b}$ is obtained from θ and ϕ through

$$\vec{b} = \begin{pmatrix} b_x \\ b_y \\ b_z \end{pmatrix} = \begin{pmatrix} \cos\phi\cos\theta \\ \sin\phi\cos\theta \\ \sin\theta \end{pmatrix} \tag{3}$$

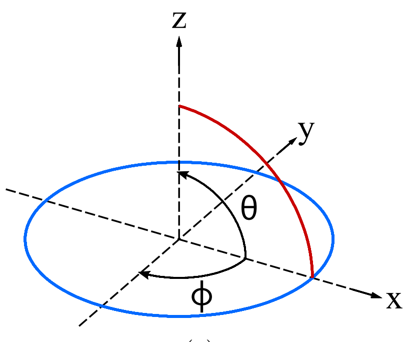

(a)

Figure 1: ϕ and θ as *azimuth*(blue) and *elevation*(red)

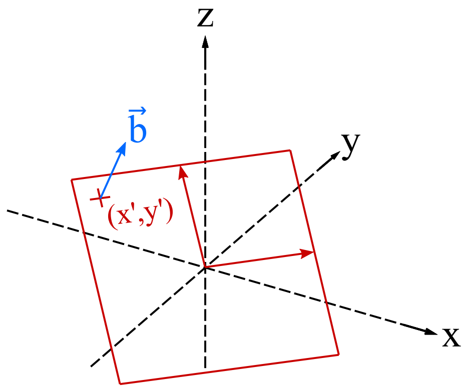

Figure 2: Line parametrisation by Roberts with x', y' (red) and the line's directional vector $\vec{b}$ (blue)

Since two anti-parallel directional vectors describe the same line, the vectors $\vec{b}$ have to be confined to a half-space for the representation to be unique. This can be achieved by restricting the angle ranges to $0 \leq \theta \leq \frac{\pi}{2}$ and $-\pi < \phi \leq \pi$. The remaining redundancy through anti-parallel vector pairs in the (x, y)-plane ($b_z = 0$) is removed with the restrictions $b_y \geq 0$ if $b_z = 0$ and $b_x = 1$ if $b_y = b_z = 0$.

When the *position* of the line is represented by an arbitrary anchor point, this leads to three parameters of which one is redundant. To remove this redundancy, Roberts first defines a plane which passes through the origin and is perpendicular to the line. The two parameters x' and y' are then defined as the coordinates of the intersection of the line and the plane in the plane's own 2D coordinate frame (see Fig 2).

From an arbitrary point $\vec{p} = (p_x, p_y, p_z)$ on the line, the parameters x' and y' are obtained with:

$$x' = \left(1 - \frac{b_x^2}{1+b_z}\right) p_x - \left(\frac{b_x b_y}{1+b_z}\right) p_y - b_x p_z \tag{4a}$$

$$y' = -\left(\frac{b_x b_y}{1+b_z}\right) p_x + \left(1 - \frac{b_y^2}{1+b_z}\right) p_y - b_y p_z \tag{4b}$$

A point $\vec{p}$ on the line can in turn be obtained with:

$$\vec{p} = x' \cdot \begin{pmatrix} 1 - \frac{b_x^2}{1+b_z} \\ -\frac{b_x b_y}{1+b_z} \\ -b_x \end{pmatrix} + y' \cdot \begin{pmatrix} -\frac{b_x b_y}{1+b_z} \\ 1 - \frac{b_y^2}{1+b_z} \\ -b_y \end{pmatrix} \tag{5}$$

To utilise this parametrisation for a 3D Hough transform, a suitable discretisation of the parameter space has to be chosen.

2.3 Parameter regularisation

The discretisation of θ and ϕ determines the orientations that can be detected by the Hough transform. A naïve approach is the uniform discretisation of the angles θ and ϕ with constant step size Δ:

$$\theta = \theta_{min} + i \cdot \Delta, \quad 0 \leq i \leq \frac{\theta_{max} - \theta_{min}}{\Delta} \tag{6a}$$

$$\phi = \phi_{min} + j \cdot \Delta, \quad 0 \leq j \leq \frac{\phi_{max} - \phi_{min}}{\Delta} \tag{6b}$$

The number of resulting direction vectors is

$$n_{uniform} = \left\lfloor \frac{(\theta_{max} - \theta_{min}) \cdot (\phi_{max} - \phi_{min})}{\Delta} \right\rfloor \tag{7}$$

A step size of $1°$, or $\Delta = \pi/180$, with $-\pi < \phi \leq \pi$ and $0 \leq \theta \leq \frac{\pi}{2}$ then yields a hemisphere consisting of 32400 directional vectors. These, however,

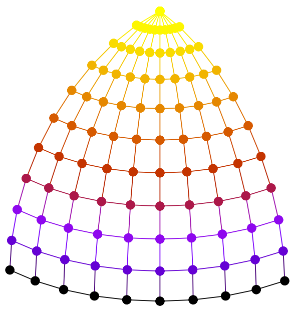

Figure 3: Quarter hemisphere of vertices obtained by uniform discretisation of ϕ and θ

are not equidistantly distributed on the hemisphere's surface (see Fig. 3). While the arc distance of adjacent vectors on the hemisphere's equator is Δ, it decreases as the elevation approaches $\pi/2$.

An accumulator array, which uses these vectors would therefore contain considerably more cells for nearly vertical lines than for lines that are almost parallel to the x-axis for example. This has the effect that the resolution for horizontal lines is much coarser than for vertical lines. The Hough transform would therefore be biased in favour of horizontal lines due to their bigger cells. In other words: this parameter space discretisation is not rotation invariant; a rotation of the point cloud input to the Hough transform would lead to different results due to the variation in angular accuracy.

In the following, we describe two different alternative methods for achieving a more homogeneous discretisation of the direction space. The aim is to achieve an equidistant distribution of directional vectors, so that the arc distances of neighbouring vector end points on the hemisphere surface are approximately constant.

Cosine-corrected discretisation of ϕ. For the uniform discretisation (6a) & (6b) with constant angle step size Δ, the nearest neighbour distance of direction vector end points with the same elevation θ is

$$d_{NN}(\theta) = \Delta \cdot \cos(\theta) \tag{8}$$

To compensate for this effect, it is natural to make the step-sizes for θ and ϕ different. When the step-size $\Delta_\theta = \Delta$ is kept constant, the step-size Δ'_ϕ for ϕ should increase with θ:

$$\Delta'_\phi(\theta) = \frac{\Delta_\theta}{\cos(\theta)} = \Delta_\theta \cdot \sec(\theta) \tag{9}$$

This approach, however, only provides a constant distance $d_{NN}(\theta) = \Delta_\theta$ in the unlikely case when Δ'_ϕ is in integer fraction of 2π. Otherwise the arc distance between ϕ_{max} and ϕ_{min} is less than Δ'_ϕ. It is thus necessary to smooth out this difference and to define the step size Δ_ϕ by

$$\Delta_\phi(\theta) = (\phi_{max} - \phi_{min}) \Bigg/ \left\lfloor \frac{\phi_{max} - \phi_{min}}{\Delta'_\phi(\theta)} \right\rfloor \tag{10}$$

Using $\Delta_\theta = \Delta$ and $\Delta_\phi(\theta)$ for discretisation yields an approximately equidistant direction sampling

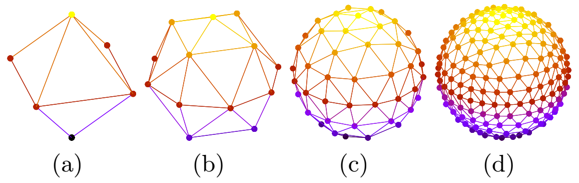

Figure 4: Octahedron after $0, 1, 2, 3$ tessellation steps

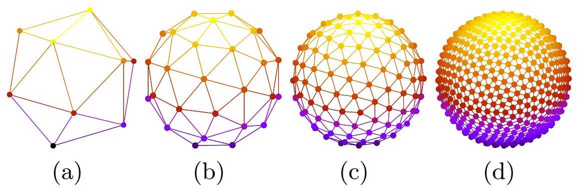

Figure 5: Icosahedron after $0, 1, 2, 3$ tessellation steps

with $d_{NN}(\theta) \approx \Delta$. The direction vectors are calculated with

$$\theta_i = \theta_{min} + i \cdot \Delta \tag{11a}$$

$$\phi_{ij} = \phi_{min} + j \cdot \Delta_\phi(\theta_i) \tag{11b}$$

$$\vec{b}_{ij} = \begin{pmatrix} \cos\phi_{ij}\cos\theta_i \\ \sin\phi_{ij}\cos\theta_i \\ \sin\theta_i \end{pmatrix} \tag{11c}$$

where

$$i = 0, 1, \ldots, \left\lfloor \frac{\theta_{max} - \theta_{min}}{\Delta_\theta} \right\rfloor$$

$$j = 0, 1, \ldots, \left\lfloor \frac{\phi_{max} - \phi_{min}}{\Delta'_\phi\,(i \cdot \Delta + \theta_{min})} \right\rfloor$$

The number of resulting direction vectors is

$$n_{coscorr} = \sum_{i=0}^{\left\lfloor \frac{\theta_{max} - \theta_{min}}{\Delta} \right\rfloor} \left\lfloor \frac{\phi_{max} - \phi_{min}}{\Delta'_\phi\,(i\Delta + \theta_{min})} \right\rfloor \tag{12}$$

A step size of $1°$ ($\Delta = \pi/180$) then yields 20763 instead of 32400 direction vectors.

The cosine-corrected discretisation (11) indeed reduces direction inhomogeneity and the size of the accumulator array. But d_{NN} is still only approximation constant, and direction vectors form an irregular pattern which leads to apparently random fluctuations of the arc distance in θ-direction. For an approximately equidistant distribution with desirable symmetry properties the tessellation of a Platonic solid is preferable.

Tesselation of a Platonic solid. In computer graphics, tessellation means the process of fragmenting a polygon into its subareas, to enable separate computation of new information and to visualise changes to the shape of the polygon.

Since graphics hardware is generally designed to process triangles, polygon triangulation is most commonly used for tessellation (Nvidia, 2010).

One use-case are *refinement-algorithms*, which use tessellation to increase the resolution of a model and smooth its surface. Then displacement mapping is used, which is much more effective on polygons with a great amount of vertices. It uses a height map to displace the polygon's vertices and can be used to create detailed surface textures. Since Version 11, Microsoft's DirectX popularly provides this technique to increase realism in 3D graphics.

Similarly a simple polyhedron can be tessellated repeatedly and its vertices be normalised to resemble a unit sphere as accurately as needed. Finally, after removing anti-parallel vectors, the resulting vertices can be used as directional vectors for the 3D Hough transform.

To obtain an almost uniform surface density and a nearly equidistant distribution of the direction vectors, it is advisable to use platonic solids as the starting point of the tessellation because of their symmetry properties. Each vertex of a platonic solid has the exact same number of neighbouring vertices and each edge between the vertices has the same length. A platonic solid therefore defines an exactly equidistant distribution of directional vectors on a sphere.

An Octahedron (see Fig. 4(a)) for example consists of eight triangles, six vertices, twelve equally long edges and is invariant under rotations by 90° around any axis. Its six vertices are defined as

$$\mathcal{O} = \{(\pm 1, 0, 0), (0, \pm 1, 0), (0, 0, \pm 1)\} \tag{13}$$

An icosahedron (see Fig. 4(a)) consists of 20 triangles, twelve vertices, 30 equally long edges and can be defined using the golden ratio φ:

$$\mathcal{I} = \{(0, \pm 1, \pm\varphi), (\pm 1, \pm\varphi, 0), (\pm\varphi, 0, \pm 1)\}$$
$$\varphi = \frac{1}{2}\left(1 + \sqrt{5}\right) \tag{14}$$

Each triangle can now be divided into four new ones using polygon triangulation by inserting a new vertex $\vec{d}$ between each pair of vertices $(\vec{a}, \vec{b})$ of the triangle and normalising its length:

division no.	*directions*	d_{NN}
1	21	0.5465
2	81	0.2794
3	321	0.1412
4	1281	0.0713
5	5121	0.0389
6	20481	0.0180

Table 1: Number of directions and nearest neighbour distance d_{NN} for subsequent icosahedron subdivisions.

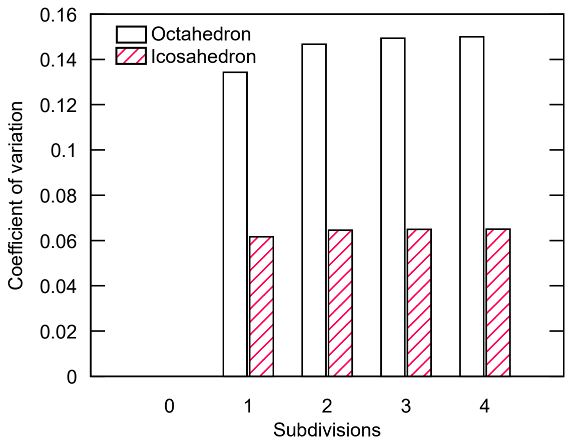

Figure 6: Coefficient of variation $c_v = \sigma/\mu$ for the length of all edges of an Octahedron and an Icosahedron after up to 4 tessellation steps

$$\vec{d} = \frac{\vec{a} + \vec{b}}{\|\vec{a} + \vec{b}\|} \tag{15}$$

Doing so for all of the polygon triangles results in a new vertex for each edge and three new edges for each new vertex:

$$|\mathcal{V}'| = |\mathcal{V}| + |\mathcal{E}| \tag{16}$$
$$|\mathcal{E}'| = 4 \cdot |\mathcal{E}| \tag{17}$$

where $\mathcal{V}$ is the set of vertices, $\mathcal{E}$ the set of edges, and $|.|$ stands for the number of elements. This can be repeated as often as necessary for the desired level of granularity. Table 1 shows the number of unique directions and the average nearest neighbour arc distances for different numbers of icosahedron subdivisions. For six subdivisions, the arc distance approximately corresponds to $1° = \pi/180 \approx 0.1745$.

It should be noted that there is only a finite number of Platonic solids, and that vertices obtained by subdivisions therefore cannot be exactly equidistantly distributed. The distance variation resulting from our method is not high, however, especially when it starts with an icosahedron, which is the Platonic with the largest number of vertices. The coefficient of variation $c_v = \sigma/\mu$ for the length of all edges of a tessellated icosahedron is much lower than that of a tessellated octahedron (see Fig. 6) which implies that it is a better approximation of an equidistant distribution.

Application to 3D Hough transform. In Algorithm 1, there is the freedom to choose which

Algorithm 2 Hough transform for 3D lines

```
Input: point cloud $X = \{\vec{x}_1, \ldots, \vec{x}_n\}$,
    direction vectors $B = \{\vec{b}_1, \ldots, \vec{b}_{N_1}\}$,
    $x'$-discretisation $X' = \{x'_1, \ldots, x'_{N_2}\}$,
    $y'$-discretisation $Y' = \{y'_1, \ldots, y'_{N_3}\}$
Output: voting array $A$ of size $N_1 \times N_2 \times N_3$
1: $A(\vec{b}_i, x'_j, y'_k) \leftarrow 0$ for all $\vec{b}_i, x'_j, y'_k$
2: for $\vec{x} \in X$ do
3:   for $\vec{b}_i \in B$ do
4:     $(x', y') \leftarrow$ computed after Eq. (4)
5:     $(x'_j, y'_k) \leftarrow$ NN to $(x', y')$ from $X' \times Y'$
6:     $A(\vec{b}_i, x'_j, y'_k) \leftarrow A(\vec{b}_i, x'_j, y'_k) + 1$
7:   end for
8: end for
9: return A
```

parameters are utilised for the predefined loops in lines 3-5, and which remaining parameters are to be computed for all values of the other predefined parameter values. In our discretisation, it is much more complicate to find the closest direction for a given direction than to find the closest x' and y' values. Consequently, the loop should go over the precomputed discrete directions and x' and y' are to be computed for each input point and each direction with Eq. (4). The resulting algorithm is listed in Algorithm 2.

3 USE CASE: RIDGE DETECTION

To test the 3D line detection, we used airborne laser scanning data of the city of Krefeld. The data was scanned with an average step size of about 24cm in the x and y direction. We combined these data with land register data in order to extract point clouds of 20 individual buildings. We extracted candidate points from each point based on local curvature and compared the eventually detected 3D lines with the expected results. The following subsections describe the extraction criterion for the candidate points and the results.

3.1 Point cloud filtering

Our criterion for filtering ridge and edge candidates was based on the observation that edge and ridge points should have a higher curvature than their neighbourhood. We estimated the curvature

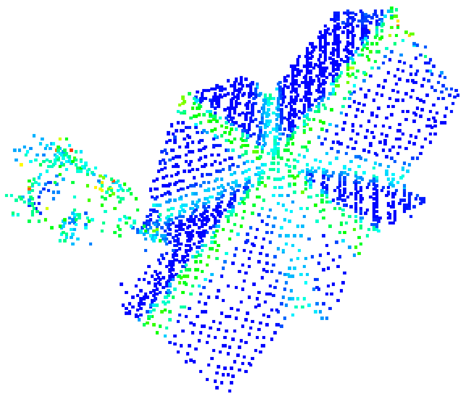
(a) Magnitude of highest eigenvalues (blue = low, red = high)

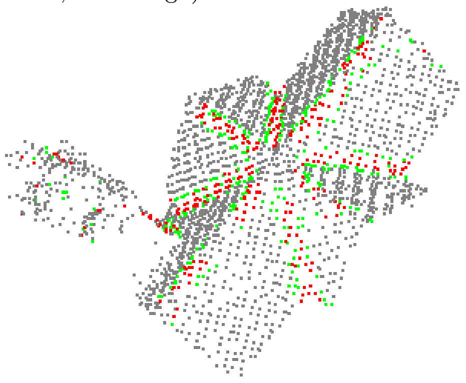
(b) Filtered candidate points (green = after global thresholding, red = after local thresholding)

Figure 7: Estimated curvature (highest eigenvalue) of a surface point cloud and the selected candidate points.

with the Point Cloud Library (PCL)[1] function *PrincipalCurvaturesEstimation*.

This function estimates as a first step the surface normal for every point with an analysis of the eigenvectors and eigenvalues of a covariance matrix created from the k nearest neighbours of the query point. In our case we used $k = 20$, because for smaller values of k the normals were too noisy and for higher values of k we observed rotated surface normals at the borderline between small surfaces. Once all surface normals have been computed, all normals from the k-neighbourhood around a query point are projected in the tangent plane. In the projected plane, the covariance matrix of the projected lines is calculated and its two eigenvalues are returned as the curvature estimation.

We used the *highest eigenvalue* as a curvature estimation. An example can be seen in Fig. 7(a).

[1]`http://pointclouds.org/`

location	n	m_{uni}	m_{reg}	*location*	n	m_{uni}	m_{reg}	*location*	n	m_{uni}	m_{reg}
Anrather	4	3	4	Glockenspitz	8	5	5	Moerser	1	1	1
Bonifatius	2	2	2	Grenz	4	2	3	Oelschlaeger	2	2	2
Buschdonk	3	2	3	Hardenberg	5	4	3	Seiden	4	3	3
Dreikoenigen	1	1	1	Huelser	6	2	5	Steckendorf	2	1	1
Evgl.Kirche	7	4	4	Ispels	9	5	7	Tannen	3	1	2
Friedr.-Ebert	7	5	7	Knein	5	1	3	Wieland	4	4	4
Gladbacher	5	2	3	Koenigs	8	4	6	*total*	90	54	69

Table 2: The number of ground truth lines (n) for roofs at different locations in our dataset, and the number of detected lines with a Hough transform with the naïve uniform discretisation (m_{uni}) and with the regularised discretisation via tessellation (m_{reg}).

On these curvature values, we first performed a global thresholding operation by selecting all points with the highest eigenvalue greater than 10% of the total maximum value and the lowest eigenvalue less than 10% of the total maximum value (green and red points in Fig. 7(b)). On these points, we then applied a local threshold by removing all points with a curvature less than the mean curvature of all $k = 20$ neighbors (red points in Fig. 7(b)).

3.2 Results

For a noisy data set of 20 complete point clouds of roofs, we have manually notated the ridges and edge lines. This lead to the numbers of ground truth lines listed in the column labelled n in Table 2. On the points clouds that have been filtered as described in section 3.1, we have applied the Hough transform with our direction tessellation as follows: the step size in the (x', y')-plane was set to 0.5, which is approximately two times the NN distance in the scanning raster, and the number of directions was set to 1281, which corresponds to four subdivisions of an icosahedron.

In the accumulator array of the Hough transform for each roof, we selected with a *non-maximum suppression* (Burger and Burge, 2009) the n (the number of ground truth lines) most voted lines and counted, how many of the ground truth lines have been detected. For the non-maximum suppression, the graph from the tesselation process was reused for neighbour relations. Two vectors $\vec{a}$ and $\vec{b}$ are neighbours, if there is an edge (a, b) in the graph. For each vertex we then defined a neighbourhood with path length $l = 4$ as every vertex that can be reached with a minimum of l edges.

The results are shown in the column labelled m_{reg} in Table 2. For comparison, we have also counted the number of correctly detected lines with the naïve uniform angle discretisation with approximately the same total number of different directions (column m_{uni} in Table 2). The new method lead to an overall detection rate of $69/90 \approx 77\%$ of the ground truth lines, while the naïve discretisation only detected $54/90 = 60\%$ of the ground truth lines. This is a clear improvement.

A closer look at the reasons for missed ground truth lines showed that in 11 cases a ground truth line showed up as two similar lines detected by the Hough transform. One example is shown in Fig. 8(a): here a single ridge shows up as two lines due to some curvature at the end. Another

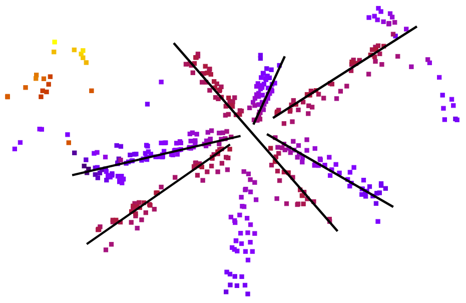
(a) Example with five of the six lines being detected. One of the ground truth lines is split up into two different detected lines.

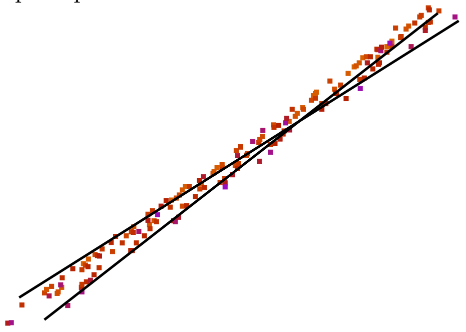
(b) Another example of a split line

Figure 8: Example Results of the 3D Hough Transform

typical example can be seen in Fig. 8(b): due to noise in the data, the ridge is not represented as a line, but as a rectangle in which the two *diagonals* are the longest lines and are thus detected by the Hough transform.

This means that of the 90 highest maxima in the Hough accumulator arrays, actually $69+11 = 80$ correspond to ground truth lines. This leads to a rate of $80/90 \approx 89\%$ lines among those returned by the Hough transform that are correct.

4 CONCLUSIONS

The presented discretisation of the direction parameters for the Hough transform for 3D line detection is a simple method to avoid an uneven distribution of directions. The method is not restricted to 3D line detection, but can be generally used for the Hough transform when parameters in the Hough space represent a direction in a 3D space, e.g. for plane detection in 3D.

The application to ridge detection shows that the new parameter space representation for 3D line detection works quite well even on very noisy data. The noise in our data was due to the very simple rules for filtering candidate points that possibly belong to ridges. Further improvements for this specific use case are to be expected when more sophisticated methods are used for candidate point selection.

In this paper, we only considered discretisation approaches that produce symmetric and regular direction patterns. It would be interesting to investigate how these compare to irregular patterns, e.g. obtained from Fibonacci numbers (González, 2010) or generalisations thereof (Anderson, 1996). The use of such patterns would however make it necessary to find a well-defined way for implementing the non-maximum suppression. In our approach, this can be done in a natural way, because the tesselation algorithm produces a neighbourship graph as a by-product.

ACKNOWLEDGEMENTS

We are grateful to the Katasteramt Krefeld for providing us with the laser scan data from Geobasisdaten der Kommunen und des Landes NRW ©Geobasis NRW 2014. Moreover, we would like to thank the anonymous reviewers for their helpful comments.

REFERENCES

Anderson, P. G. (1996). Advances in linear pixel shuffling. In Bergum, G., Philippou, A., and Horadam, A., editors, *Applications of Fibonacci Numbers*, pages 1–21. Springer, Netherlands.

Bhattacharya, P., Liu, H., Rosenfeld, A., and Thompson, S. (2000). Hough-transform detection of lines in 3-D space. *Pattern Recognition Letters*, 21(9):843–849.

Burger, W. and Burge, M. (2009). *Principles of Digital Image Processing - Core Algorithms.* Springer, London.

González, A. (2010). Measurement of areas on a sphere using Fibonacci and latitude-longitude lattices. *Mathematical Geosciences*, 42(1):49–64.

Hough, P. V. (1962). Method and means for recognizing complex patterns. US Patent 3,069,654.

Ishida, Y., Izuoka, H., Chinthaka, H., Premachandra, N., and Kato, K. (2012). A study on plane extraction from distance images using 3D Hough transform. In *Soft Computing and Intelligent Systems (SCIS) and International Symposium on Advanced Intelligent Systems (ISIS)*, pages 812–816.

Moqiseh, A. and Nayebi, M. (2008). 3-D Hough transform for surveillance radar target detection. In *IEEE Radar Conference RADAR '08*, pages 1–5.

Mukhopadhyay, P. and Chaudhuri, B. B. (2015). A survey of Hough transform. *Pattern Recognition*, 48(3):993–1010.

Nvidia (2010). NVIDIA GF100: World's fastest GPU delivering great gaming performance with true geometric realism. `http://www.nvidia.com/object/IO_86775.html`.

Qiu, W., Yuchi, M., Ding, M., Tessier, D., and Fenster, A. (2013). Needle segmentation using 3D Hough transform in 3D TRUS guided prostate transperineal therapy. *Medical physics*, 40(4):042902.

Roberts, K. (1988). A new representation for a line. In *Computer Vision and Pattern Recognition CVPR'88*, pages 635–640.

Schenk, T. (2004). From point-based to feature-based aerial triangulation. *ISPRS Journal of Photogrammetry and Remote Sensing*, 58(5):315–329.

Zhou, H., Qiu, W., Ding, M., and Zhang, S. (2008). Automatic needle segmentation in 3D ultrasound images using 3D improved Hough transform. In *Medical Imaging*, page 691821.